Topological action potentials in engineered tissues

Hillel Ori[1], Marc Duque Ramirez[1], Rebecca Frank Hayward[2], He Tian[1], Gloria Ortiz[3], Adam E. Cohen[1,4,*]

[1] Department of Chemistry and Chemical Biology, Harvard University, Cambridge, MA 02138
[2] School of Engineering and Applied Science, Harvard University, Cambridge, MA 02138
[3] Department of Chemistry, University of California, Berkeley, CA 94720
[4] Department of Physics, Harvard University, Cambridge, MA 02138

*cohen@chemistry.harvard.edu

Abstract

Due to the nonlinear current-voltage relations of ion channels, an interface between two tissues can have very different bioelectrical properties compared to either tissue on its own. Here we show that gap junction-coupled interfaces between non-excitable tissues can be excitable. This topologically protected excitability occurs over a far larger range of ion channel expression levels than does excitability in the bulk. Topological excitations at tissue interfaces can cause local elevations in calcium concentration, possibly providing a bioelectrical mechanism for interface sensing. As in condensed matter physics, topological excitations in electrophysiology constitute a distinct class of phenomena which may show exotic and novel properties.

Introduction

The Schrödinger equation of quantum mechanics[1], the Turing reaction-diffusion equations of chemical patterning[2], and the Hodgkin-Huxley equations of electrophysiology[3] all have similar mathematical structures: they are first order in time, second order in space, and have a possibly nonlinear reaction-like term. One thus expects similar classes of dynamics in these physically very different domains.

Topological excitations in solid-state systems are an emerging area of basic research and applied interest.[4] These excitations arise from the requirement that the wavefunction must be continuous across an interface, even when the band structure changes. Membrane potential in electrophysiology plays a role analogous to wavefunction in quantum mechanics. Across a gap junction-coupled interface between tissues with different resting potentials, the voltage must go through all intermediate values, possibly including regions where the membrane potential would be unstable in the bulk. This continuity requirement could lead to novel topologically protected excitations at tissue interfaces. If two non-excitable tissues are brought into contact, can the interface become excitable? Engineered and patterned cells have been a powerful tool for dissecting intercellular molecular signaling cascades,[5,6] but despite some theoretical work,[7,8] this approach has not previously been applied experimentally to bioelectrical signaling.

Historically, spatial structures in bioelectrical signaling have been difficult to study because patch clamp measurements probed the voltage at only a single point in space. Recent advances in voltage imaging[9,10] opened the door to studying the spatial structures of bioelectrical excitations. By combining patterned optogenetic stimulation and high-speed voltage imaging, one can probe the excitability of a complex

tissue as a function of space and time. This approach has been used to identify new types of bioelectrical excitations in engineered tissues,[11] and also to map bioelectrical signals throughout embryonic development.[9,12] Here we map the excitability at interfaces between non-excitable engineered tissues and observe topologically stabilized action potentials. Detailed numerical simulations and a simple analytical model capture the key features of these excitations. These findings suggest new mechanisms of bioelectrical signaling that may arise in native tissues.

Results

Human Embryonic Kidney (HEK293) cells become electrically excitable when genetically engineered to express an inward-rectifier potassium channel (e.g. $K_{ir}2.1$ or $K_{ir}2.3$) and a voltage-gated sodium channel (e.g. $Na_V1.3$,[13] $Na_V1.5$[14], or $Na_V1.7$[15]). When grown in a confluent monolayer, endogenous gap junctions introduce nearest-neighbor coupling, which can then support propagating electrical waves. If the cells further express a blue light-activated cation channel such as CheRiff[16] and either express a far-red voltage indicator protein[10] or are labeled with a red-shifted voltage-sensitive dye[17], then one can optically induce action potentials and simultaneously map their propagation through the engineered tissue.[11,14,18]

First, we explored whether the sodium and potassium channels needed to be in the same cells. We made separate pools of HEK cells that expressed CheRiff and either $Na_V1.5$ alone or $K_{ir}2.1$ alone (Fig. 1A). We mixed the cell populations and mapped the voltage in confluent monolayer cultures using the far-red voltage-sensitive dye BeRST1 (Methods).[17] Localized optogenetic stimulation evoked action potentials which propagated radially outward (Fig. 1B, Movie 1). In cultures expressing either $Na_V1.5$ or $K_{ir}2.1$ alone, optical activation of CheRiff did not lead to action potentials or wave propagation (Fig. S1). These results show that a mixture of non-excitable cells can become excitable by sharing currents through gap junctions.

Next, we used a thin plastic divider to physically separate the $Na_V1.5$- and the $K_{ir}2.1$-expressing cells on opposite halves of the culture dish (Fig. 1C, Methods). Fluorescent tags marked the two populations (Fig. 1D). After the cells had settled, we gently removed the divider and let the cells migrate to fill the gap (Methods). This approach led to a clean interface with the two cell populations on opposite sides.

Optogenetic stimulation of either population alone did not evoke action potentials. Remarkably, optogenetic stimulation with a stripe that spanned the interface induced electrical excitations which propagated along the interfacial line without entering the bulk on either side (Fig. 1E, Movie 2). The spikes had a width of 0.76 ± 0.15 mm transverse to the interface, a length of 2.21 ± 0.62 mm along the interface, and propagated at 12.9 ± 3.5 mm/s (mean ± s.d., n = 5 samples, Fig. 2A). Thus, topological action potentials can arise between non-excitable tissues. For control experiments, we made interfaces in which one cell population expressed either $Na_V1.5$ or $K_{ir}2.1$, and the adjoining population expressed neither channel. These interfaces were not excitable, confirming the necessity of both ion channels on opposite sides of the interface (Fig. S2A,B). Furthermore, in dishes where the $Na_V1.5$ and $K_{ir}2.1$-expressing cells had not yet fully closed the gap, topological action potentials propagated only in regions where the two cell types had come into contact (Fig. S2C).

To better understand our results, we simulated a conductance-based model of our experiment using established parameters for $K_{ir}2.1$ and $Na_V1.5$[11,19] (Supplementary Model 1). This model reproduced the basic phenomena, showing interface-localized action potential initiation and propagation (Fig. 2B, Movie 3). We then simulated the effect of changes in the expression level of the gap junctions, $Na_V1.5$ or $K_{ir}2.1$. Modulating the gap junction conductance, G_{gj}, changed the width, length, and conduction speed of the topological action potential, with all three parameters scaling as $(G_{gj})^{1/2}$, as one would expect from dimensional analysis (Fig. S3). Topological action potentials arose over at least a 60-fold variation in g_{Na} and at least a 1000-fold variation in g_K, persisting to the highest levels of g_K and g_{Na} simulated (Fig. 2C).

We then performed analogous simulations where the $Na_V1.5$ and $K_{ir}2.1$ were homogeneously distributed through all cells. For cells co-expressing both ion channels, excitability occurred over a much narrower range of expression levels (~30-fold in $Na_V1.5$, but only ~3-fold in $K_{ir}2.1$; Fig. 2C). In the case of homogeneous expression, excitability required a delicate balance of depolarizing (Na_V, leak, channelrhodopsin) and polarizing (K_{ir}) currents to drive all the phases of the action potential. In contrast, in the interfacial structure, gap junction-mediated currents caused the relative contributions of Na_V and K_{ir} to vary from 0 to 100% transverse to the interface, dramatically expanding the range of parameters which supported excitability (Fig. 2D).

To facilitate an understanding of the basic requirements for topological action potentials, we developed a simplified model inspired by the FitzHugh-Nagumo (FHN) model (Supplementary Model 2; Supplementary Code).[20,21] We broke the characteristic N-shaped nonlinearity of the FHN model into two components: one approximated the shape of a Na_V current-voltage (*I-V*) curve, and one approximated the shape of a K_{ir} *I-V* curve. These two components, each active in only one half-space, each had a single zero-crossing and hence a single stable resting potential. At the interface where both currents contributed, the *I-V* curve had three zero crossings and hence could support nonlinear excitations (Fig. S4). The simplified FHN-like model reproduced our observed propagating topological action potentials (Fig. 2E). Changes to the model parameters also yielded many other types of topological excitations, with diverse voltage patterns in space and time (Fig. S5C-E; Movie 4). These observations suggest that tissue interfaces might support a rich repertoire of novel bioelectrical phenomena.

We then explored experimentally the interaction of interface topology and sample topology. Using a plastic drinking straw as a separator, we plated $Na_V1.5$-expressing cells in a disk and $K_{ir}2.1$-expressing cells in the surrounding region (Fig. 3, Methods). Optical stimulation in a line across the interface evoked topological action potentials which propagated bidirectionally around the interface, annihilating each other when they collided. To evoke a directional wave, we applied a tonic stimulation with a line to create a thin zone of Na_V channel inactivation. We then turned off the tonic stimulation and stimulated briefly to one side of this zone. This stimulus protocol created an action potential propagating in only one direction. The inactivated Na_V channels recovered by the time the action potential completed one trip around the disk. Thereafter the action potential propagated around the interface, circulating stably for many minutes (Fig S6; Movie 5). These results demonstrate that topological action potentials can sense the topology of tissue boundaries and can store information via their handedness of circulation.

In the presence of voltage-gated Ca^{2+} channels, topological excitations might lead to locally elevated Ca^{2+}, which could then turn on downstream patterns of gene expression. First, we tested whether co-expression of a T-type calcium channel, $Ca_V3.2$, and $K_{ir}2.3$ in HEK cells were sufficient, on their own, to support action potential propagation. We used HEK cells with constitutive expression of $K_{ir}2.3$, doxycycline-inducible expression of $Ca_V3.2$,[22] and lentiviral expression of CheRiff for optogenetic stimulation. We induced $Ca_V3.2$ expression with doxycycline and then mapped the voltage in confluent monolayer cultures of these cells (Fig. S7A). Local optogenetic stimulation induced action potentials which propagated radially outward and then broke up into self-sustaining spiral waves (Movie 6). Incubation with the Ca_V blocker nifedipine abolished the excitability (Fig. S7B). Samples where $Ca_V3.2$ expression was not induced were also not excitable (Fig. S7C). Together, these results establish that $Ca_V3.2$ and K_{ir} 2.3 are sufficient to sustain propagating action potentials in confluent HEK cell monolayers.

We then asked whether topological action potentials could arise at the interface between cells expressing $Ca_V3.2$ and cells expressing $K_{ir}2.1$. As with the Na_V channels, optogenetic stimulation with a stripe that spanned the interface induced excitations in membrane voltage which propagated along the interface (Fig. 4A, Movie 7). In separate samples, we used a far-red calcium-sensitive dye (Methods) and observed propagating Ca^{2+} signals along the interface too (Fig 4B, Movie 8). These results show that topological action potentials can be driven by multiple types of depolarizing channels (Na_V, Ca_V) and can drive increases in intracellular Ca^{2+} in cells within an electrical coupling length of a tissue interface.

Discussion

The nonlinear behavior of ion channels, together with gap junctional sharing of currents, gives tissue interfaces unique excitability properties different from the bulk. Here we showed that mixtures of non-excitable cells can be excitable; an interface between non-excitable tissues can be excitable; a circular tissue interface can support stably circulating topological excitations; and topological excitations can drive local elevations in Ca^{2+} concentration.

The existence of topological action potentials at tissue interfaces raises the possibility of other types of topological effects in electrophysiology. For instance, our numerical simulations predicted a regime in which a $Na_V1.5$-$K_{ir}2.1$ interface showed spontaneous spiking, whereas cells co-expressing $Na_V1.5$ and $K_{ir}2.1$ did not show spontaneous spiking under any conditions. Other combinations of ion channels could lead to additional topological effects. For instance, expression of pacemaker channels on one side of the interface might lead to spontaneous spiking that starts only when two tissues touch, providing a means to signal first contact. Depending on the other ion channels on both sides of the interface, these contact-evoked spikes could either propagate just along the interface, into the bulk on one side, or into the bulk on both sides. Topological electrophysiology mechanisms could enable cells to sense the presence of nearby tissue interfaces, to determine the topology of their tissue environment, or to communicate over long distances.

The ways in which bioelectrical signaling complements chemical signaling pathways in embryonic development and morphogenesis[12,23] are still being worked out. It is not yet known whether topological excitations arise in native tissues. Recent work has highlighted the importance of voltage-gated Ca^{2+}

channels in development.[24–26] These effects occur in nominally non-excitable cells, though our results highlight that excitability is not an intrinsic feature of a cell but rather depends on the surrounding tissues. Interactions between zebrafish skin melanophores and xanthophores also suggest a contact-dependent bioelectrical signaling mechanism.[27] Our results suggest that analyses of such effects should not just examine the properties of individual cell types, but should also consider tissue interfaces as distinct electrophysiological entities. Finally, we note that due to the parallel structure of the Hodgkin-Huxley and Turing reaction diffusion equations, analogous interfacial excitations could also occur in chemical reaction-diffusion systems.

Acknowledgments

This work was supported by the Vannevar Bush Faculty Fellowship (A.E.C.) and an EMBO Fellowship to H.O (ALTF 543-2020). We thank Noam Ziv and his laboratory for hosting H.O. during the COVID-19 pandemic. We thank Terrance Snutch for helpful discussions and for providing cells expressing $Ca_V3.2$ and $K_{ir}2.3$. We thank Evan Miller for the BeRST1 dye. We thank Vincenzo Vitelli, Colin Scheibner and Suyang Xu for helpful discussions. We thank Shahinoor Begum, Andrew Preecha, Tamar Galateanu and Lonya Odessky for technical assistance.

Methods

Cell line generation and culture

Cells stably co-expressing $Na_V1.5$ and CheRiff-eGFP were described in Ref [15]. For cells expressing $K_{ir}2.1$ and CheRiff, cells constitutively expressing CheRiff were transiently transfected with pCAG-Kir2.1-T2A-tdTomato (from Massimo Scanziani, Addgene 60598) using CalFectin transfection reagent (SignaGen Laboratories) following manufacturer's directions. Cells were seeded in imaging plates 24-48 hours after transfection. Cell culture maintenance was the same as for Optopatch Spiking HEK cells[18]. Cells stably expressing human $Ca_V3.2$, along with cells constitutively expressing $K_{ir}2.3$ and doxycycline inducible $Ca_V3.2$ were a generous gift from Terrance Snutch and are described in Ref. [22]. These cells were infected with a lentiviral vector expressing pCMV-CheRiff-CFP (Addgene 136636) to render them light sensitive.

Sample preparation

35 mm dishes with 14 mm glass coverslip bottoms (Cellvis, #D35-14-1.5-N) were coated with polyethyleneimine (PEI). Two days prior to imaging, linear interfaces were created by seeding $Na_V1.5$- and $K_{ir}2.1$-expressing cells separated by a 100 µm thick plastic divider, 4×10^5 cells of each type. After 2 h, the divider was carefully removed, the plate was gently washed with phosphate-buffered saline (PBS) to remove unattached cells, the plate was incubated in culture medium. For the circular interfaces, the central island was created by seeding 5×10^5 $Na_V1.5$-expressing cells inside a region defined by a circular 5 mm diameter plastic cylinder (a cut drinking straw). After 2 h, the cylinder was removed, unattached cells were removed by gentle washing with PBS, and the plate was incubated overnight with culture medium. Approximately 10^6 $K_{ir}2.1$-expressing cells were then seeded onto the dish. The $K_{ir}2.1$ cells primarily attached in the annular region not already occupied by $Na_V1.5$-expressing cells.

Imaging and stimulation

For voltage imaging, cells were washed to remove culture medium and then incubated with 1-2 µM BeRST1 dye in PBS for 30 min in a tissue culture incubator. Immediately before imaging, samples were washed twice and immersed in imaging solution containing (in mM) 125 NaCl, 15 HEPES, 25 glucose, 2.5 KCl, 1 $MgCl_2$, 2 $CaCl_2$ with pH adjusted to 7.3 with NaOH. Sample preparation for Ca^{2+} imaging was similar, except that the cells were washed and incubated with 3 µM BioTracker™ 609 Red Ca^{2+} AM Dye (EMD Millipore #SCT021) in PBS for 30 min in a tissue culture incubator, then washed and immersed in imaging solution. Widefield imaging was performed using an Axiovert 200 (Zeiss) inverted microscope, equipped with a light source (xenon arc, XBO 75 W) and filter sets for the GFP, tdTomato, BeRST1 and calcium dye channels. Light was collected using a 2X, numerical aperture 0.1 objective lens (ThorLabs #TL2X-SAP) into an EMCCD camera (Andor iXon EM+ 897, 512x512 pixels, 35 frames/s). The field of view (FOV) was expanded to 9.9 mm in the sample plane by placing a 0.5X image reducer (View Solutions, #MA513302) in the light collection path. CheRiff was excited by a 470 nm LED (ThorLabs #M470L4-C4) connected to the topside illumination path. The stimulation region was defined by a thin slit inserted in the excitation beam and projected onto the sample plane via the microscope condenser. The camera was controlled via the Andor SOLIS software. The LED illumination was controlled via a National Instruments DAQ card. Camera and LED were synchronized using a custom Matlab code. For imaging and patterned optogenetic stimulation of $Ca_V3.2$- $K_{ir}2.3$ monolayers and $Ca_V3.2$-$K_{ir}2.1$ interfaces we used an ultrawidefield microscope as, described in Ref. [28].

Data analysis

All data were processed and analyzed using custom software (MATLAB). The baseline fluorescence, *F*, of the BeRST1 signal was calculated for each pixel by the mean intensity over the time series. The movie was then converted into units of ΔF/F and smoothed by spatially filtering with a 12x12 pixels kernel.

For the linear interface experiments (Fig. 1) 10 consecutive trials were averaged before converting to ΔF/F units. To calculate the spatial shape of the propagating AP (Fig. 2A), images acquired at different times were laterally shifted to cancel the motion of the AP wavefront. Background noise from variation between rows was suppressed by setting pixels below the 20th percentile of their row to the minimum intensity of the frame. Finally, the movie was averaged along time with a 12 frames window.

Kymographs were constructed by averaging rectangles of 40x10 pixels along the interface.

For the circular interface experiment (Fig. 3) the time series of the ΔF/F movie was reconstructed from a detrended vectorized ΔF/F sequence to account for changes in baseline signal due to photobleaching. In addition to spatial filtering movies were averaged along time with a 6 frame sliding window. For the time trace plot (Fig. 3D) a spatial region of interest was defined and averaged across pixels.

GFP and tdTomato images (Fig. 1A,B) were processed by subtracting a background image (no illumination) and dividing pixel-wise by a reference image (dish with no cells) to account for spatial variations in illumination intensity. A gamma correction was applied to the tdTomato image to permit visualization of cells with widely varying expression levels.

Numerical modeling

Model equations and simulation methods can be found in Supplementary Models 1 and 2, and Supplementary Code.

Figures

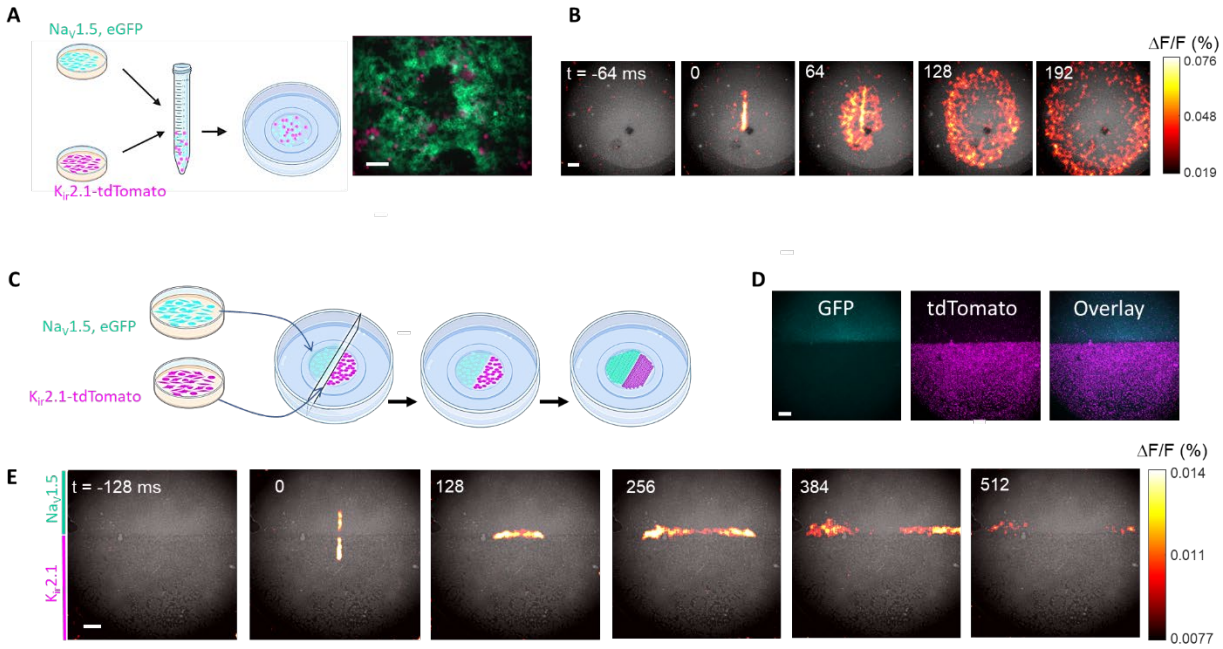

Figure 1. Topological action potentials arise at interfaces of non-excitable tissues. A,B) A mixture of non-excitable cells can be excitable. A) Left: sample preparation. HEK cell lines were engineered to express either $K_{ir}2.1$ (an inward-rectifier K^+ channel) or $Na_V1.5$ (a voltage-gated Na^+ channel). All cells also expressed a light-gated ion channel, CheRiff. The two populations were mixed, plated, and grown to form a gap junction-coupled monolayer. Right: Distribution of $Na_V1.5$-expressing cells (tagged with a GFP marker) and $K_{ir}2.1$-expressing cells (tagged with a tdTomato marker). Expression is mutually exclusive. B) Montage of frames from voltage imaging movie (Movie 1). The monolayer was stimulated by a short pulse of blue light (vertical bar at $t = 0$). Changes in voltage were then monitored via the fluorescence of the far-red voltage-sensitive dye BeRST1 (baseline signal in gray, $\Delta F/F$ in color). Optogenetic stimulation evoked outward propagating action potentials. C-E) Topological action potential at interfaces. C) Sample preparation. HEK cells expressing $K_{ir}2.1$ or $Na_V1.5$ were plated on opposite sides of a thin plastic divider. After removal of the divider, the cells migrated to fill the gap and formed a gap junction-coupled interface. D) Interface between populations of $Na_V1.5$-expressing cells (tagged with GFP) and $K_{ir}2.1$-expressing cells (tagged with tdTomato). C) Montage of frames from a voltage-imaging movie (Movie 2). Optogenetic stimulation spanning the interface at $t = 0$ evoked a topological action potential that propagated outward solely along the interface (baseline signal in gray, $\Delta F/F$ in color). Scalebars: A) 0.1 mm; B,D,E) 1 mm. See also Figs. S1, S2.

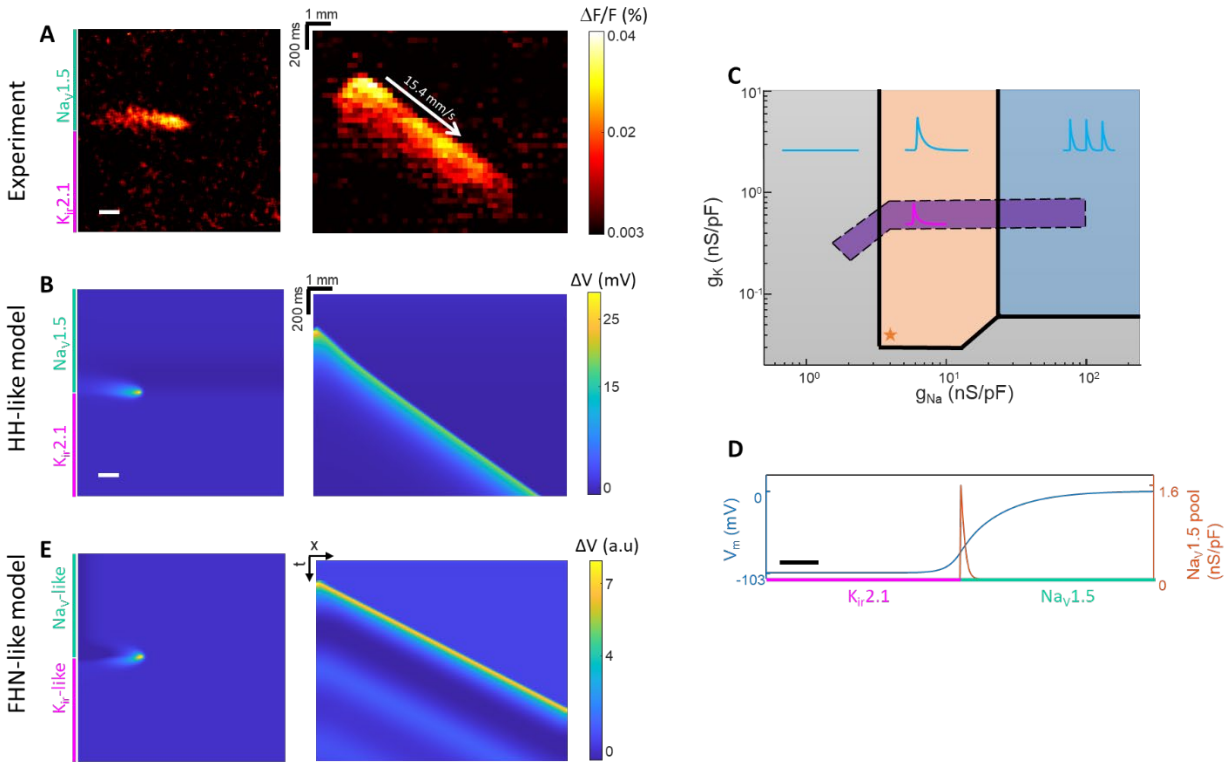

Figure 2. Quantification and numerical simulations of topological action potentials. A) Left: spatial profile of a topological action potential. Right: kymograph constructed by averaging transverse to the interface, showing topological action potential propagation. B) Numerical simulations of an interface between a $K_{ir}2.1$-expressing cell population (g_K = 0.04 nS/pF, E_K = -107 mV) and a $Na_V1.5$-expressing cell population (g_{Na} = 3.9 nS/pF, E_{Na} = 75 mV). Left: Image of a topological action potential propagating along a tissue interface. Color scale corresponds to deviation from local resting potential. Right: kymograph showing topological action potential propagation (Movie 3). C) Calculated phase diagram of excitability of $K_{ir}2.1$-$Na_V1.5$ interface. The parameter space is divided into non-excitable, excitable, and spontaneously active phases. The purple region indicates the excitable phase of a homogenous system, where each cell expresses both $Na_V1.5$ and $K_{ir}2.1$ channels. The interfacial system has a spontaneously active phase (blue region) which is absent in the homogenous system. Orange star corresponds to the parameters used for the simulations in (B). D) Steady-state resting voltage and sodium channel availability along a line perpendicular to the interface. The voltage varies continuously between a polarized state on the $K_{ir}2.1$ side and a depolarized state on the $Na_V1.5$ side. The available reserve of $Na_V1.5$ conductance ($g_{Na} \times (1 - m^3)\, h$) has a peak near the interface. The band of high $Na_V1.5$ reserve supports AP propagation. Scale bar 0.2 mm. (E) Numerical simulation of simplified FHN-like model of topological action potentials (see Supplementary Model 2 for details). Left: Image of a topological action potential propagating along a tissue interface. Right: kymograph showing topological action potential propagation (Movie 4). See also Figs. S3-S5.

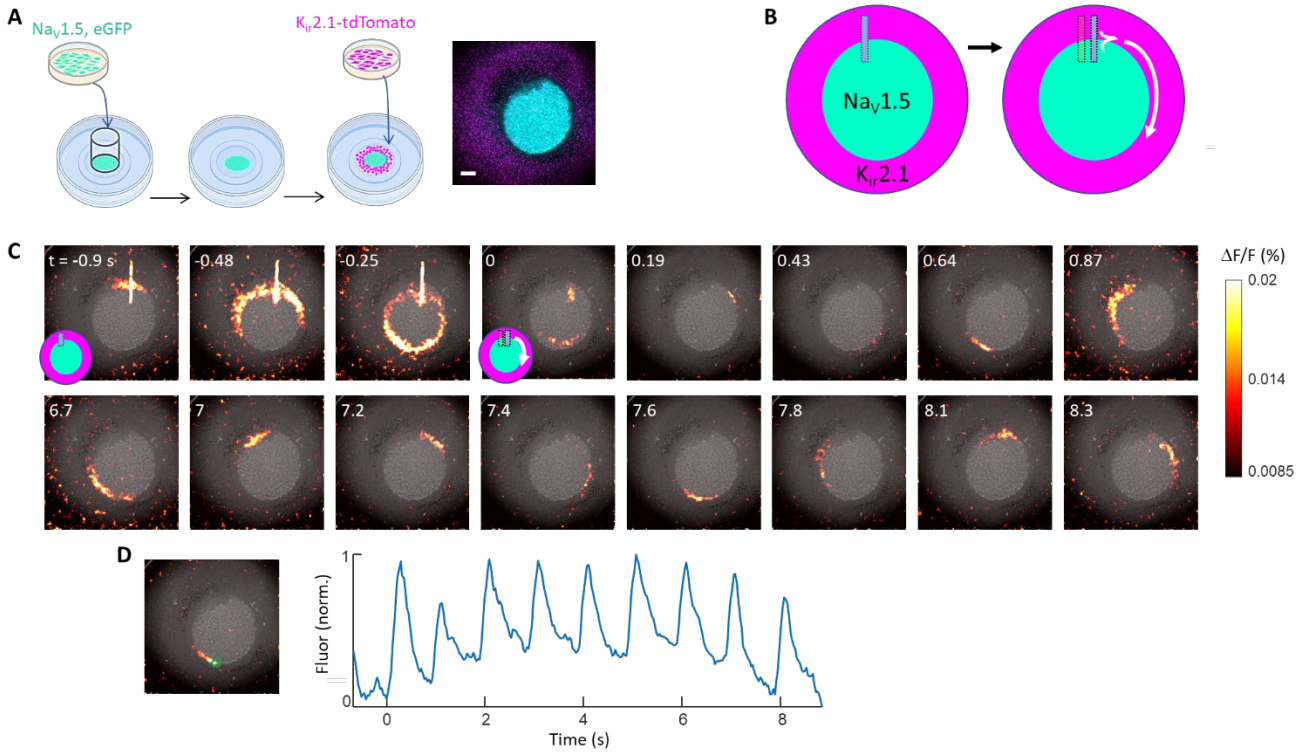

Figure 3. Persistently propagating topological action potentials at a circular interface. A) Sample preparation. HEK cells expressing Na$_V$1.5 and CheRiff were seeded into circular region defined by a thin plastic cylinder. HEK cells expressing K$_{ir}$2.1 and CheRiff were then added and settled in the unoccupied periphery. B) Stimulation protocol for evoking a unidirectional topological action potential wave. A long (450 ms) illumination pulse was delivered to a portion of the interface, to drive local Na$_V$1.5 inactivation. A short (~30 ms) pulse was then delivered to a nearby interface region, evoking a topological action potential that propagated unidirectionally. By the time the action potential completed one cycle, the inactivated Na$_V$ channels had recovered, permitting cyclical propagation. C) Montage showing application of the inactivation stimulus, the trigger stimulus, and persistent AP propagation along the interface. D) Time-dependent fluorescence in the region indicated by the green polygon, showing a persistently propagating topological action potential. Scalebars: 1 mm. See also Fig. S6; Movie 5.

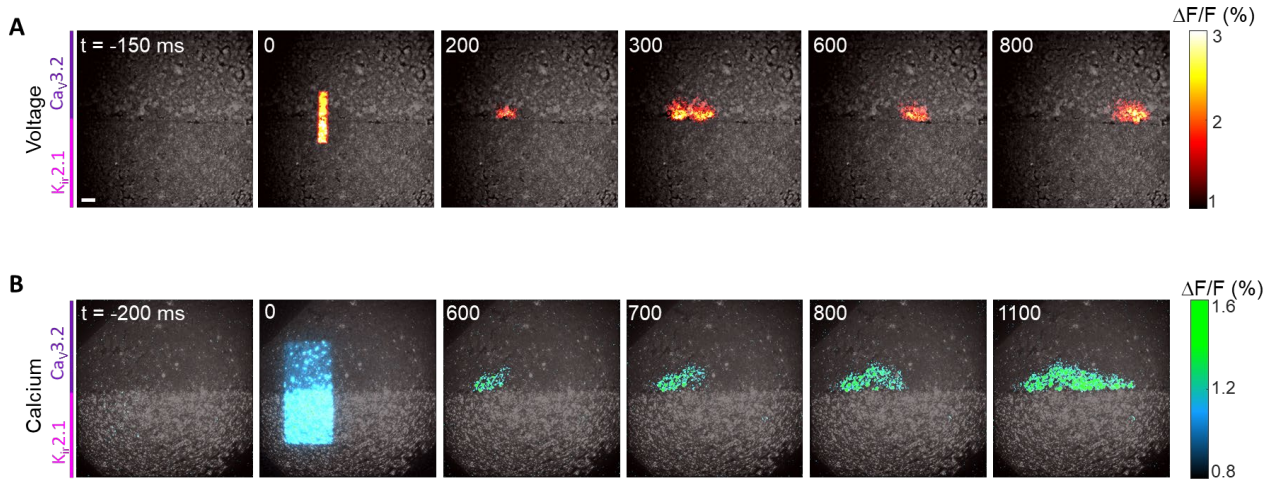

Figure 4. Topological action potentials driven by Ca^{2+} currents. A) Montage of frames from a voltage-imaging movie (Movie 7). Optogenetic stimulation spanning the interface at t = 0 evoked a topological action potential that propagated outward solely along the interface. B) Montage of frames from a calcium-imaging movie (from a different sample, Movie 8). Optogenetic stimulation at the interface evoked a calcium signal that propagated along the interface. Scale bar 1 mm. Baseline signal in gray, $\Delta F/F$ in color. See also Fig. S7.

References

1. Schrödinger, E. An Undulatory Theory of the Mechanics of Atoms and Molecules. *Phys. Rev.* **28**, 1049–1070 (1926).
2. Turing, A. M. The chemical basis of morphogenesis. *Philos. Trans. R. Soc. Lond. B Biol. Sci.* **237**, 37–72 (1952).
3. Hodgkin, A. L. & Huxley, A. F. A quantitative description of membrane current and its application to conduction and excitation in nerve. *J. Physiol.* **117**, 500–544 (1952).
4. Hasan, M. Z. & Kane, C. L. Colloquium: Topological insulators. *Rev. Mod. Phys.* **82**, 3045–3067 (2010).
5. Ma, Y. *et al.* Synthetic mammalian signaling circuits for robust cell population control. *Cell* **0**, (2022).
6. Warmflash, A., Sorre, B., Etoc, F., Siggia, E. D. & Brivanlou, A. H. A method to recapitulate early embryonic spatial patterning in human embryonic stem cells. *Nat. Methods* **11**, 847–854 (2014).
7. Cervera, J., Levin, M. & Mafe, S. Bioelectrical Coupling of Single-Cell States in Multicellular Systems. *J. Phys. Chem. Lett.* **11**, 3234–3241 (2020).
8. Xu, J. *et al.* The Role of Cellular Coupling in the Spontaneous Generation of Electrical Activity in Uterine Tissue. *PLOS ONE* **10**, e0118443 (2015).
9. Hou, J. H., Kralj, J. M., Douglass, A. D., Engert, F. & Cohen, A. E. Simultaneous mapping of membrane voltage and calcium in zebrafish heart in vivo reveals chamber-specific developmental transitions in ionic currents. *Front. Physiol.* **5**, 344 (2014).
10. Adam, Y. *et al.* Voltage imaging and optogenetics reveal behaviour-dependent changes in hippocampal dynamics. *Nature* **569**, 413 (2019).
11. McNamara, H. M. *et al.* Bioelectrical domain walls in homogeneous tissues. *Nat. Phys.* **16**, 357–364 (2020).
12. Levin, M. Bioelectric signaling: Reprogrammable circuits underlying embryogenesis, regeneration, and cancer. *Cell* **184**, 1971–1989 (2021).
13. Park, J. *et al.* Screening fluorescent voltage indicators with spontaneously spiking HEK cells. *PloS One* **8**, e85221 (2013).
14. McNamara, H. M., Zhang, H., Werley, C. A. & Cohen, A. E. Optically controlled oscillators in an engineered bioelectric tissue. *Phys. Rev. X* **6**, 031001 (2016).
15. Zhang, H., Reichert, E. & Cohen, A. E. Optical electrophysiology for probing function and pharmacology of voltage-gated ion channels. *eLife* **5**, e15202 (2016).
16. Hochbaum, D. R. *et al.* All-optical electrophysiology in mammalian neurons using engineered microbial rhodopsins. *Nat. Methods* **11**, 825–833 (2014).
17. Huang, Y. L., Walker, A. S. & Miller, E. W. A photostable silicon rhodamine platform for optical voltage sensing. *J. Am. Chem. Soc.* **137**, 10767–10776 (2015).
18. McNamara, H. M. *et al.* Geometry-dependent arrhythmias in electrically excitable tissues. *Cell Syst.* **7**, 359-370. e6 (2018).
19. ten Tusscher, K. H. W. J., Noble, D., Noble, P. J. & Panfilov, A. V. A model for human ventricular tissue. *Am. J. Physiol.-Heart Circ. Physiol.* **286**, H1573–H1589 (2004).

20. FitzHugh, R. Impulses and physiological states in theoretical models of nerve membrane. *Biophys. J.* **1**, 445–466 (1961).
21. Nagumo, J., Arimoto, S. & Yoshizawa, S. An active pulse transmission line simulating nerve axon. *Proc. IRE* **50**, 2061–2070 (1962).
22. Belardetti, F. *et al.* A Fluorescence-Based High-Throughput Screening Assay for the Identification of T-Type Calcium Channel Blockers. *ASSAY Drug Dev. Technol.* **7**, 266–280 (2009).
23. Gregor, T., Tank, D. W., Wieschaus, E. F. & Bialek, W. Probing the Limits to Positional Information. *Cell* **130**, 153–164 (2007).
24. Pitt, G. S., Matsui, M. & Cao, C. Voltage-Gated Calcium Channels in Nonexcitable Tissues. *Annu. Rev. Physiol.* **83**, 183–203 (2021).
25. Atsuta, Y., Tomizawa, R. R., Levin, M. & Tabin, C. J. L-type voltage-gated Ca2+ channel CaV1.2 regulates chondrogenesis during limb development. *Proc. Natl. Acad. Sci.* **116**, 21592–21601 (2019).
26. Lin, S.-S. *et al.* Cav3.2 T-type calcium channel is required for the NFAT-dependent Sox9 expression in tracheal cartilage. *Proc. Natl. Acad. Sci.* **111**, E1990–E1998 (2014).
27. Inaba, M., Yamanaka, H. & Kondo, S. Pigment pattern formation by contact-dependent depolarization. *Science* **335**, 677 (2012).
28. Werley, C. A., Chien, M.-P. & Cohen, A. E. Ultrawidefield microscope for high-speed fluorescence imaging and targeted optogenetic stimulation. *Biomed. Opt. Express* **8**, 5794–5813 (2017).